Assessing the efficiency of free energy calculation methods

ARTICLE *in* THE JOURNAL OF CHEMICAL PHYSICS · MARCH 2004

Impact Factor: 2.95 · DOI: 10.1063/1.1642607 · Source: PubMed

3 AUTHORS, INCLUDING:

Eric Darve
Stanford University
100 PUBLICATIONS **2,342** CITATIONS
SEE PROFILE

Andrew Pohorille
162 PUBLICATIONS **5,871** CITATIONS
SEE PROFILE

Assessing the efficiency of free energy calculation methods

David Rodriguez-Gomez[a] and Eric Darve[b]
Department of Mechanical Engineering, Stanford University, California 94305

Andrew Pohorille[c]
Exobiology Branch, MS 239-4, NASA Ames Research Center, Moffett Field, California 94305

(Received 20 August 2003; accepted 24 November 2003)

The efficiencies of two recently developed methods for calculating free energy changes along a generalized coordinate in a system are discussed in the context of other, related approaches. One method is based on Jarzynski's identity [Phys. Rev. Lett. **78**, 2690 (1997)]. The second method relies on thermodynamic integration of the average force and is called the adaptive biasing force method [Darve and Pohorille, J. Chem. Phys. **115**, 9169 (2001)]. Both methods are designed such that the system evolves along the chosen coordinate(s) without experiencing free energy barriers and they require calculating the instantaneous, unconstrained force acting on this coordinate using the formula derived by Darve and Pohorille. Efficiencies are analyzed by comparing analytical estimates of statistical errors and by considering two numerical examples—internal rotation of hydrated 1,2-dichloroethane and transfer of fluoromethane across a water-hexane interface. The efficiencies of both methods are approximately equal in the first but not in the second case. During transfer of fluoromethane the system is easily driven away from equilibrium and, therefore, the performance of the method based on Jarzynski's identity is poor. © *2004 American Institute of Physics.* [DOI: 10.1063/1.1642607]

I. INTRODUCTION

Estimating how free energy changes with the state of a system occupies a central place in applications of statistical mechanics to problems of chemical or biological interest. From these free energy changes it is possible, for example, to establish which states of the system are stable, what are their probabilities, and how the equilibria between these states are influenced by external conditions. Free energies are also of great utility in determining kinetics of transitions between different states.

A variety of methods have been developed to compute free energies of condensed phase systems.[1–6] In this paper, we focus on one class of methods—those that allow for calculating free energy changes along one or several generalized coordinates in the system, often called ''reaction coordinates.'' A variety of interesting problems can be formulated, at least approximately, in these terms. Examples vary from conformational equilibria and associations of small molecules to partition coefficients between immiscible liquids, receptor-drug interactions, protein-protein and protein-DNA associations, stability of small proteins,[5,7,8] or response of a polymer to an external force.[9–15] In some cases only the free energy difference between the end points is being sought whereas in other instances the full free energy profile is of interest.

Considering that in almost all cases of practical interest a significant computational effort is required to determine free energy changes it is hardly surprising that efficiencies (or, for a fixed cost, accuracies) of different methods are of great concern. Several properties of the system, such as the rate of diffusive motion along the reaction coordinate or equilibration of the system along other degrees of freedom, can influence these efficiencies. In many cases, however, the main difficulty in the efficient calculation of the free energy is associated with its shape along the reaction coordinate. If the free energy changes markedly along this coordinate, Boltzmann sampling of its different values becomes highly nonuniform. This, in turn, may have considerable detrimental effect on the performance of many methods for calculating free energies.

Several approaches have been proposed to overcome this difficulty.[1,3,4,16,17] Recently, two methods have been developed that allow for recovering the free energy profile from trajectories, in which sampling along the reaction coordinate is exactly or approximately uniform. One method is based on Jarzynski's equality[18,19] and requires generating a series of appropriate nonequilibrium trajectories that describe evolution of the system along the reaction coordinate. The other method, called adaptive biasing force, relies on thermodynamic integration of the average force acting on the reaction coordinate during unconstrained simulations.[20,21] Considering that neither of the two methods experiences difficulties associated with nonuniform sampling of the reaction coordinates, it might be expected that their application should provide an efficient mean for estimating free energies. We explore this point in detail by comparing formulas for statistical error in both methods and by examining specific numerical examples.

[a]Also at Center for Turbulence Research, NASA Ames Research Center, Moffett Field, CA 94305. Electronic mail: davidrg@stanford.edu
[b]Electronic mail: darve@stanford.edu
[c]Also at Department of Pharmaceutical Chemistry, University of California, San Francisco, CA 94143.
Electronic mail: dpohorill@ raphael.arc.nasa.gov

In the next section, we briefly review the theory underlying the methods in the context of other, related approaches also used in this study. We recall the previously obtained formulas for statistical error in Jarzynski's method[22,23] and derive the formula for the same quantity in the adaptive biasing force. We illustrate the difference between these formulas in a simple example of a one-dimensional harmonic oscillator. Next, we apply both methods to two specific examples—conformational equilibria in 1,2-dichloroethane in water and transfer of fluoromethane across a water-hexane interface. The reaction coordinates are, respectively, the Cl–C–C–Cl torsional angle and the distance between the centers of mass of the solute and the hexane lamella along the normal to the interface. In both cases, accurate free energy profiles have been obtained previously[20,24,25] and served as the reference. As will be shown, both methods are approximately equally efficient in the first but not in the second case. The paper closes with a brief summary and conclusions regarding the efficiency of both methods in the calculations of free energies.

TABLE I. Notation frequently used in the article.

k_B	Boltzmann constant
T	Temperature
β	$1/(k_BT)$
Z	Canonical partition function
$\mathbf{x}$	Cartesian coordinates
$\xi(\mathbf{x})$	Generalized coordinate
$\mathbf{p_x}$	Conjugate momenta of $\mathbf{x}$
H	Hamiltonian
$\langle S\rangle_N$	Arithmetic average of $\{S_1,\ldots,S_N\}$
$\mathrm{E}[S],\overline{S}$	Expectation of S
$\mathrm{SD}[S],\sigma_S$	Standard deviation of S
$\mathrm{Var}[S],\sigma_S^2$	Variance of S
$S\sim N(\overline{S},\sigma_S^2)$	Random variable S has a normal distribution with expectation $\overline{S}$ and variance σ_S^2
$P(S)$	Probability density function of S
ΔA	Free energy difference
K	Total number of molecular dynamics steps used to estimate ΔA
$\Delta A^{(\mathrm{C})}$	Constraint force estimate of the free energy
F_ξ^c	Effective force acting on ξ in constrained simulations
$\Delta A^{(\mathrm{abf})}$	Adaptive biasing force estimate of the free energy
F_ξ^u	Effective force acting on ξ in unconstrained simulations
$\Delta A_N^{(\mathrm{J})}$	Jarzynski's free energy estimator
$\Delta A_N^{(\mathrm{G})}$	Free energy estimator for Gaussian distribution of work
τ	Switching time of a fast growth trajectory
N	Number of fast growth trajectories
L	Number of time steps per fast growth trajectory

II. THEORY

A. Numerical calculation of free energies

In this section we outline methods for computing free energy differences ΔA that are further used in this paper. We start with the most straightforward methods based on computing probability density functions and move on to more advanced methods, such as the adaptive biasing force method of Darve and Pohorille,[20,21] which deals with numerical difficulties caused by the presence of energy barriers. We conclude with the methods applicable to out of equilibrium simulations recently developed by Jarzynski[18,19,26] and Crooks.[27–30] We will point out that the latter class of methods has some drawbacks and, in particular, becomes inaccurate for molecular systems which are easily driven out of equilibrium. This point will be developed in more details in the rest of the article. In Table I, we summarize the notation most frequently used in this article.

For a system at constant temperature T, constant volume V, and with a constant number of particles M, the Helmholtz free energy $A(M,V,T)$ is given by

$$A(M,V,T) = -k_BT\log Z(M,V,T),$$

where Z is the canonical partition function and k_B is the Boltzmann constant. From a computational standpoint, calculating $A(M,V,T)$ involves the difficult task of computing a volume in phase space. A more feasible objective is to compute free energy differences. For example, if we define a reaction coordinate ξ, which is a function of the particle positions $\mathbf{x}$, we can represent the free energy as a function of M, V, T, and $\xi(\mathbf{x})$:

$$A(M,V,T,\xi_0) = -k_BT\log\frac{\int \exp[-\beta H(\mathbf{x},\mathbf{p_x})]\,\delta(\xi(\mathbf{x})-\xi_0)d\mathbf{x}\,d\mathbf{p_x}}{\Lambda^{3M}M!} \quad (1)$$

where Λ is the thermal wavelength and $\beta=1/(k_BT)$. Then the free energy difference between $\xi=\xi_a$ and $\xi=\xi_b$ is defined as

$$\begin{aligned} A(M,V,T,\xi_b)-A(M,V,T,\xi_a) &= \Delta A_{a\to b} \\ &= -k_BT\log\frac{\int \exp[-\beta H(\mathbf{x},\mathbf{p_x})]\,\delta(\xi(\mathbf{x})-\xi_b)d\mathbf{x}\,d\mathbf{p_x}}{\exp[-\beta H(\mathbf{x},\mathbf{p_x})]\,\delta(\xi(\mathbf{x})-\xi_a)d\mathbf{x}\,d\mathbf{p_x}}. \end{aligned} \quad (2)$$

A straightforward approach to estimating $\Delta A_{a\to b}$ consists in observing that the probability density function $P(\xi_a)$ is defined by

$$P(\xi_a) = \frac{\int \exp[-\beta H(\mathbf{x},\mathbf{p_x})]\,\delta(\xi(\mathbf{x})-\xi_a)d\mathbf{x}\,d\mathbf{p_x}}{\int \exp[-\beta H(\mathbf{x},\mathbf{p_x})]d\mathbf{x}\,d\mathbf{p_x}}.$$

$P(\xi_b)$ is defined similarly. Then

$$\Delta A_{a\to b} = -k_BT\log\frac{P(\xi_b)}{P(\xi_a)}.$$

To estimate the ratio of the probabilities we need to know the probability density $P(\xi)$ in the range $[\xi_a,\xi_b]$, which can be computed from a molecular dynamics (MD) or Monte Carlo simulation. There are several difficulties that might arise. If the state corresponding to ξ_a is much more stable than the state $\xi=\xi_b$, then the system will be poorly sampled at ξ_b. If there is a high energy barrier separating ξ_a from ξ_b, transitions between these two states will be rare, yielding large errors in the numerical estimate of $\Delta A_{a\to b}$.

To remedy these difficulties, several approaches have been considered. The most common method relies on the observation that $\Delta A_{a\to b}$ can be obtained from the following, more general equation:

$$\Delta A_{a\to b}=U_B(\xi_b)-U_B(\xi_a)-k_BT\log\frac{\int\exp\{-\beta[H(\mathbf{x},\mathbf{p_x})-U_B(\xi)]\}\delta(\xi(\mathbf{x})-\xi_b)d\mathbf{x}\,d\mathbf{p_x}}{\int\exp\{-\beta[H(\mathbf{x},\mathbf{p_x})-U_B(\xi)]\}\delta(\xi(\mathbf{x})-\xi_a)d\mathbf{x}\,d\mathbf{p_x}},$$

where H is the Hamiltonian of the system, $\mathbf{p_x}$ are conjugate momenta of $\mathbf{x}$, and $U_B(\xi)$ is an external potential applied to the system. If $U_B(\xi)$ is a good approximation of $A(\xi)$ then the sampling over ξ becomes almost uniform as

$$\frac{\int\exp\{-\beta[H(\mathbf{x},\mathbf{p_x})-U_B(\xi)]\}\delta(\xi(\mathbf{x})-\xi_b)d\mathbf{x}\,d\mathbf{p_x}}{\int\exp\{-\beta[H(\mathbf{x},\mathbf{p_x})-U_B(\xi)]\}\delta(\xi(\mathbf{x})-\xi_a)d\mathbf{x}\,d\mathbf{p_x}}=\frac{\exp[-\beta A(\xi_b)]}{\exp[-\beta U_B(\xi_b)]}\frac{\exp[-\beta U_B(\xi_a)]}{\exp[-\beta A(\xi_a)]}\approx 1.$$

Although this method has been effectively used for a wide variety of problems it also has an important drawback in that a good initial guess of $A(\xi)$ is required to get an efficient sampling of ξ. This implies that we need to have a good, *a priori* understanding of a system under study. Otherwise, the improvement in sampling efficiency would be small or none.

Sampling can be further improved by splitting the computation into several, partially overlapping ranges (''windows'') along ξ, the union of which covers the entire interval $[\xi_a,\xi_b]$.[31] It can be shown that the computational cost decreases as $1/n_w$, where n_w is the number of windows. The optimal number of windows is reached when the characteristic times needed to sample one interval along ξ and the coordinates orthogonal to ξ are comparable. A point of difficulty is that the data in each window need to be shifted by a constant in order to obtain a continuous energy profile along ξ.[32,33] This can become a source of error if there are many intervals or they do not sufficiently overlap.

1. Thermodynamic integration methods

Thermodynamic integration methods are based on the observation that

$$\Delta A_{a\to b}=\int_{\xi_a}^{\xi_b}\frac{dA(\xi)}{d\xi}d\xi.$$

Using Eq. (1), one can prove that

$$\Delta A_{a\to b}=\int_{\xi_a}^{\xi_b}\left\langle\frac{\partial H(\xi)}{\partial\xi}\right\rangle_{\xi^*}d\xi^*, \tag{3}$$

where the partial derivative is computed with any set of generalized coordinates. The notation $\langle\,\rangle_{\xi^*}$ stands for an average computed over the set $\{(\mathbf{x},\mathbf{p_x}),\xi(\mathbf{x})=\xi^*\}$. One approach to estimating the integral in Eq. (3) is to constrain the system at several locations $\xi=\xi^*$ and compute the average $\langle\partial H(\xi)/\partial\xi\rangle_{\xi^*}$ at each location. This should be done with care because the conjugate momentum of ξ in a constrained simulation is also constrained. In fact, the correct, general formula for calculating $\langle\partial H(\xi)/\partial\xi\rangle_{\xi^*}$ has been derived only relatively recently.[20,21,34] In brief, we need to introduce a set of generalized coordinates $\mathbf{q}^{\xi^*}$ and conjugate momenta $\mathbf{p}^{\xi^*}$ to describe the set $\{(\mathbf{x},\mathbf{p_x}),\xi(\mathbf{x})=\xi^*,\dot\xi=0\}$. The integral becomes

$$\left\langle\frac{\partial H(\xi)}{\partial\xi}\right\rangle_{\xi^*}=\frac{\int\frac{\partial H(\xi)}{\partial\xi}\exp[-\beta H(\mathbf{q}^{\xi^*},\mathbf{p}^{\xi^*})]d\mathbf{q}^{\xi^*}d\mathbf{p}^{\xi^*}dp^*}{\int\exp[-\beta H(\mathbf{q}^{\xi^*},\mathbf{p}^{\xi^*})]d\mathbf{q}^{\xi^*}d\mathbf{p}^{\xi^*}dp^*}, \tag{4}$$

where p^* is the conjugate momentum of ξ^*. In can be shown[20,21] that with an appropriate choice of coordinates the Hamiltonian takes the form

$$H=\frac{1}{2}\frac{(p^*)^2}{m_\xi}+\frac{1}{2}(\mathbf{p}^{\xi^*})^tM_q^{-1}\mathbf{p}^{\xi^*}+U(\mathbf{q}^{\xi^*}),$$

where m_ξ and M_q are the generalized masses associated with the generalized coordinates and U is the potential energy of the system. In particular, m_ξ is defined by

$$\frac{1}{m_\xi}=\sum_{k=1}^{3M}\frac{1}{m_k}\left(\frac{\partial\xi}{\partial x_k}\right)^2,$$

where m_k are the masses of the M particles and x_k, $1\leqslant k\leqslant 3M$, are their coordinates.

The integration over p^* in Eq. (4) yields

$$\int\exp\left(-\beta\frac{1}{2}\frac{(p^*)^2}{m_\xi}\right)dp^*=\sqrt{\frac{2\pi}{\beta}}\sqrt{m_\xi}.$$

We use this result to eliminate p^* in Eq. (4):

$$\left\langle\frac{\partial H(\xi)}{\partial\xi}\right\rangle_{\xi^*}=\frac{\int\frac{\partial H(\xi)}{\partial\xi}\sqrt{m_\xi}\exp[-\beta H(\mathbf{q}^{\xi^*},\mathbf{p}^{\xi^*})]d\mathbf{q}^{\xi^*}d\mathbf{p}^{\xi^*}}{\int\sqrt{m_\xi}\exp[-\beta H(\mathbf{q}^{\xi^*},\mathbf{p}^{\xi^*})]d\mathbf{q}^{\xi^*}d\mathbf{p}^{\xi^*}}. \tag{5}$$

Therefore for a constrained simulation we have to compute the following average:

$$\frac{\left\langle\sqrt{m_\xi}\frac{\partial H(\xi)}{\partial\xi}\right\rangle_c}{\langle\sqrt{m_\xi}\rangle_c}\qquad\left(=\left\langle\frac{\partial H(\xi)}{\partial\xi}\right\rangle_{\xi^*}\right),$$

where $\langle\,\rangle_c$ denotes an average computed with $\xi=\xi^*$ and $\dot\xi=0$. The partial derivative of H with respect to ξ is complicated to calculate because of the apparent necessity to define generalized coordinates. There is, however, an alternative

that is computationally more tractable.[20,21] For simulations with a constraint, we define an effective force acting on ξ as

$$F_{\xi}^{c}=-\lambda+\frac{1}{2\beta}\sum_{k=1}^{3M}\frac{1}{m_k}\frac{\partial\xi}{\partial x_k}\frac{\partial m_{\xi}}{\partial x_k}, \tag{6}$$

where λ is the Lagrange multiplier used in SHAKE or RATTLE,[35] to impose the constraint on ξ. Then

$$\left\langle\frac{\partial H(\xi)}{\partial\xi}\right\rangle_{\xi*}=-\frac{\langle\sqrt{m_{\xi}}F_{\xi}^{c}\rangle_c}{\langle\sqrt{m_{\xi}}\rangle_c}.$$

The constrained method has some drawbacks. The number of points along ξ and the spacing between them has to be properly chosen for each system to reduce errors arising from numerical integration in Eq. (3). Perhaps more importantly, constraining ξ might cause ergodicity problems in sampling degrees of freedom orthogonal to ξ.

An alternative approach, recently proposed by Darve and Pohorille,[20,21] relies on calculating $\langle\partial H/\partial\xi\rangle_{\xi}$ using an unconstrained simulation. Then, the following effective force acting on ξ is defined:

$$F_{\xi}^{u}=m_{\xi}\frac{d^2\xi}{dt^2}+\frac{1}{\beta}\sum_{k=1}^{3M}\frac{1}{m_k}\frac{\partial\xi}{\partial x_k}\frac{\partial m_{\xi}}{\partial x_k}. \tag{7}$$

Note that the factor of 1/2 in Eq. (6) is no longer present. Then

$$\left\langle\frac{\partial H(\xi)}{\partial\xi}\right\rangle_{\xi*}=-\langle F_{\xi}^{u}\rangle_{\xi*}. \tag{8}$$

To efficiently sample ξ, even if high energy barriers are present, an external force along ξ is applied to the system. No *a priori* estimate of the biasing force is required. In the simplest implementation, the adaptive biasing force applied to the system is equal and opposite to the running average of F_{ξ}:

$$\langle F_{\xi}^{u}\rangle_{\xi,n}=\frac{\Sigma_{i=1}^{n}F_{\xi,i}^{u}}{n}.$$

To underscore this feature the method is called the adaptive biasing force (ABF) method. As the external force converges to $-\langle F_{\xi}^{u}\rangle_{\xi}$ sampling along ξ becomes uniform. In practice, convergence is quite rapid, especially if more refined estimates of $-\langle F_{\xi}^{u}\rangle_{\xi,n}$ are employed for small n.

The ABF method shares common features with both the probability method and the constrained thermodynamic integration. As in the latter method, $\Delta A_{a\to b}$ is obtained by integrating the average force acting along ξ. As in the probability method, the simulation is performed in windows but without the need to keep ξ fixed. Furthermore, the bias added to the force asymptotically converges to the "ideal" $dU_B(\xi)/d\xi$. However, the ABF method is quite different from the adaptive biasing potential approach.[16,17] To adjust U_B it is necessary to sample the whole window sufficiently well so that an improved estimate of the biasing potential in this window is obtained. Furthermore, a good initial guess for $U_B(\xi)$ is still needed. Otherwise, some regions of ξ will be sampled poorly or not at all. In contrast, the estimate for the biasing force in the ABF method is obtained locally without the need to sample the rest of the window or to have an initial guess for U_B.

2. Nonequilibrium simulations

The last category of methods that will be discussed in this paper bears some resemblance to the ABF method. In these methods, an external force is applied along ξ to change (switch) its value from ξ_a to ξ_b. Under appropriate conditions it is possible to compute $\Delta A_{a\to b}$ from the work required to perform this switch. More precisely, if one starts a simulation with $\xi=\xi_a$ and changes ξ reversibly from ξ_a to ξ_b, the following equation applies:

$$\Delta A_{a\to b}=\int_0^{\infty}\dot{\xi}\frac{\partial H(\xi)}{\partial\xi}dt.$$

We can then write

$$\Delta A_{a\to b}=W_{\infty},$$

where W_{∞} is the work required to switch with an infinitely slow velocity. This is the "slow-growth" method.

In a real simulation, however, ξ is changed at a finite, rather than infinitely small, speed. In this case, the relation between the work and the change of the free energy is only approximate,

$$\Delta A_{a\to b}\approx W_{\tau},$$

where τ is the switching time. In fact, the second law of thermodynamics imposes a bound,

$$\Delta A_{a\to b}\leqslant\overline{W_{\tau}}, \tag{9}$$

where the overbar denotes an average over trajectories at a given finite switching time τ. The error can be reduced by increasing τ, but this also increases the computational expense.

This approximation can be replaced by an exact equality using a nonequilibrium free energy expression derived by Jarzynski[18,19] and further developed by Crooks.[28–30] Let us suppose that a certain velocity profile $v_{\xi}^{0}(t)=d\xi/dt$ is chosen and that we perform several trajectories where $d\xi/dt$ is constrained and equal to $v_{\xi}^{0}(t)$. In this case,

$$\exp(-\beta\Delta A_{a\to b})=\overline{\exp(-\beta W_{\tau})}, \tag{10}$$

where the average, denoted again by the overbar, is computed over all the trajectories. This method is sometimes referred to as the "fast-growth" method. The simplest choice for $v_{\xi}^{0}(t)$ is to consider a switching at constant velocity $[v_{\xi}^{0}(t)=\text{const}]$. It is possible in general to improve the efficiency of the method by choosing a nonconstant velocity profile $v_{\xi}^{0}(t)$. In particular, in the intervals where large nonequilibrium effects are generated, the velocity $v_{\xi}^{0}(t)$ should be chosen small. Vice versa, in the intervals where the system remains close to equilibrium, it is possible to choose a large $v_{\xi}^{0}(t)$ so that the computational expense is reduced.

A remarkable feature of Eq. (10) is that the switching time τ is arbitrary. This means that in principle $\Delta A_{a\to b}$ can be accurately estimated from the set of work values $\{W_{\tau,1},W_{\tau,2},\ldots,W_{\tau,n},\ldots\}$, providing that the number of tra-

jectories, n, is sufficiently large. This is true even for short switching times, for which the system is driven far from equilibrium, and the work performed during a single simulation gives a poor estimate of the free energy difference. The nonequilibrium nature of Eq. (10) makes it appealing for calculating free energies not only from computer simulations but also from experiments. Good examples are single-molecule pulling experiments,[13,36,37] in which the micromanipulation of the molecule of interest (typically DNA, RNA, or a protein) perturbs the system irreversibly. In this case, Eq. (10) yields an estimate of the free energy change in the unfolding reaction from the irreversible pulling trajectories.

To calculate the average in Eq. (10), N trajectories are initiated at $\xi=\xi_a$. The starting configurations for these trajectories are sampled from the canonical ensemble at the desired temperature T and should be statistically independent. If we choose a constant switching velocity, we have

$$\dot{\xi}=\frac{\xi_b-\xi_a}{\tau},$$

where τ is the desired switching time. In order to enforce the proper constraint on ξ along the trajectory, which is $\dot{\xi}(t)=\dot{\xi}(0)$, we use a modified version of RATTLE described in Ref. 20.

In the rest of the paper, we will simplify the notation by abbreviating $\Delta A_{a\to b}=\Delta A$ and $W_\tau=W$. In order to simplify the presentation, we consider the case of a constant switching velocity only. However all the results can be extended to an arbitrary $v_\xi^0(t)$.

B. Numerical error of free energy formulas

In this section, we deal with the numerical error associated with the adaptive biasing force and fast-growth methods.

First, we derive a formula to assess the statistical error in the ABF that takes into account correlations between consecutive samples of F_ξ^u. We show that, under quite general assumptions, this statistical error behaves as $K^{-1/2}$, where K is the total number of time steps in the simulation.

For fast growth, we consider two different free energy formulas. One is based on the nonequilibrium relation in Eq. (10). The estimator

$$\Delta A_N^{(\mathrm{J})}=-\beta^{-1}\log\left(\frac{e^{-\beta W_1}+\cdots+e^{-\beta W_N}}{N}\right) \tag{11}$$

gives the exact value ΔA when $N\to\infty$,

$$\lim_{N\to\infty}\Delta A_N^{(\mathrm{J})}=\Delta A,$$

provided that the set of values $\{W_1,W_2,\ldots,W_N\}$ are obtained from independent simulations, with initial conditions sampled randomly from the canonical ensemble corresponding to the system at $\xi=\xi_a$. We shall refer to $\Delta A_N^{(\mathrm{J})}$ as *Jarzynski's estimator*. A major drawback of this technique is that, for finite N, the estimate contains a systematic bias.[19,22,26,27,38] In this case, the expectation of $\Delta A_N^{(\mathrm{J})}$ exceeds ΔA,

$$\mathrm{E}[\Delta A_N^{(\mathrm{J})}]>\Delta A.$$

Due to the nonlinearity of Eq. (11), the accurate evaluation of the systematic bias and statistical error of $\Delta A_N^{(\mathrm{J})}$ is difficult, especially if σ_W is much larger than k_BT. However, when the distribution of works $P(W)$ is Gaussian and $\exp(\beta^2\sigma_W^2)-1\ll N$, it is possible to give reliable estimates of both quantities.

The second fast-growth estimator under consideration was introduced by Jarzynski[26] and Hummer.[38] The authors observed that the estimator $\Delta A_N^{(\mathrm{J})}$ is biased, even when $P(W)$ is Gaussian. In this case, however, it is possible to construct an unbiased estimator[38] $\Delta A_N^{(\mathrm{G})}$:

$$\Delta A_N^{(\mathrm{G})}=\langle W\rangle_N-\frac{\beta}{2}s^2,$$
$$\langle W\rangle_N=\frac{1}{N}\sum_{i=1}^{N}W_i,\quad s^2=\frac{1}{N-1}\sum_{i=1}^{N}(W_i-\langle W\rangle_N)^2, \tag{12}$$

instead of $\Delta A_N^{(\mathrm{J})}$. This is possible because the exact free energy in the Gaussian case is given by

$$\Delta A=\overline{W}-\frac{\beta}{2}\sigma_W^2 \tag{13}$$

and

$$\mathrm{E}(\langle W\rangle_N)=\overline{W},\quad \mathrm{E}(s^2)=\sigma_W^2\ .$$

Not only is $\Delta A_N^{(\mathrm{G})}$ an unbiased estimator of ΔA but the exact expression for the variance of $\Delta A_N^{(\mathrm{G})}$ is available. From this expression it follows that, for small $\beta\sigma_W$, the error is asymptotically on the order of $K^{-1/2}$. We shall see in Sec. IV that, in practice, the applicability of $\Delta A_N^{(\mathrm{G})}$ is somewhat limited, as deviations of $P(W)$ from a Gaussian distribution can result in a considerable loss of accuracy of the estimator.

This theoretical analysis and the numerical tests presented in Secs. II C and IV will lead us to the following conclusion: For a wide class of systems, the methods based on computing free energies from the average of the instantaneous force offer higher or, at worst, comparable accuracy for the same computational cost as fast growth. In addition, estimating the error of ΔA obtained from the former methods is much easier.

1. Error in adaptive biasing force method

To approximate the integral

$$\Delta A=-\int_{\xi_a}^{\xi_b}\langle F_\xi^u\rangle_{\xi^*}d\xi^*$$

obtained by combining Eqs. (3) and (8) a quadrature rule is first applied, using nodes $\{\xi_i\}_{i=1}^p\subset[\xi_a,\xi_b]$. For the sake of simplicity, we assume that they are equally spaced:

$$\xi_i=\xi_a+\left(i-\frac{1}{2}\right)\Delta\xi,\quad \forall i=1,\ldots,p,\quad \Delta\xi=\frac{\xi_b-\xi_a}{p},$$

and the midpoint rule is applied, yielding

$$\Delta A\approx-\Delta\xi\sum_{i=1}^{p}\langle F_\xi^u\rangle_{\xi_i}. \tag{14}$$

Next, we assume that $\langle F_\xi^u\rangle_{\xi_i}$ is the expectation value with respect to the probability distribution $P(F_{\xi_i}^u)$ according to

which the forces collected in the bin $[\xi_i-\Delta\xi/2,\xi_i+\Delta\xi/2]$ are distributed. Let us denote by n_i the number of forces collected in that bin at the end of the simulation and $K=n_1+\cdots+n_p$ the total number of samples. $\{F_\xi(t_m)\}_{m=1}^K$ designates the sequence of forces computed during the entire simulation; to specify the set of forces collected in the ith bin, we write $\{F_\xi(t_l^i)\}_{l=1}^{n_i}$. The instants $\{t_l^i\}_{l=1}^{n_i}$ are not necessarily consecutive, as ξ takes values in different bins during the MD simulation. We denote the expectation and variance of the forces in the ith bin as

$$\mu_i=-\frac{\partial A}{\partial\xi}(\xi_i)=\mathrm{E}[F_{\xi_i}^u],\quad \sigma_i^2=\mathrm{Var}[F_{\xi_i}^u].$$

As we pointed out in Sec. II A, the adaptive biasing force approach is conceived to achieve asymptotically a uniform sampling along ξ. Thus,

$$\lim_{K\to\infty}P(\xi_i)=\lim_{K\to\infty}\frac{n_i}{K}=\frac{1}{p},\quad \forall\ \ i=1,...,p.$$

In particular, $n_i\to\infty$ as time goes to ∞. Then, assuming ergodicity, the running averages

$$\langle F_\xi^u\rangle_{\xi_i,n_i}=\frac{\Sigma_{l=1}^{n_i}F_\xi^u(t_l^i)}{n_i},\quad 1\leqslant i\leqslant p,$$

give an accurate estimate of μ_i as the simulation proceeds, yielding the following finite-time estimate of the free energy:

$$\Delta A^{(abf)}=-\Delta\xi\sum_{i=1}^{p}\langle F_\xi^u\rangle_{\xi_i,n_i}. \tag{15}$$

Two sources of error are found in Eq. (15):

$$\begin{aligned}|\Delta A-\Delta A^{(abf)}|&\leqslant|\Delta A-\mathrm{E}[\Delta A^{(abf)}]|\\&\quad+|\mathrm{E}[\Delta A^{(abf)}]-\Delta A^{(abf)}|\\&=E_1+E_2.\end{aligned}$$

Notice that

$$\mathrm{E}[\Delta A^{(abf)}]=-\Delta\xi\sum_{i=1}^{p}\mu_i=\Delta\xi\sum_{i=1}^{p}\frac{\partial A}{\partial\xi}(\xi_i). \tag{16}$$

Thus, we find that E_1 is the quadrature error introduced by the midpoint rule:

$$E_1=\left|\Delta A-\Delta\xi\sum_{i=1}^{p}\frac{\partial A}{\partial\xi}(\xi_i)\right|.$$

For large K the bin size can be made sufficiently small that the quadrature error becomes negligibly small.

On the other hand, E_2 represents the statistical error of estimating $\mathrm{E}[\Delta A^{(abf)}]$ from K MD steps. We will focus on this error.

We estimate the expected squared error rather than the expected value of E_2. This is justified by the Schwarz inequality:[39]

$$\begin{aligned}\mathrm{E}[E_2]&=\mathrm{E}[|\Delta A^{(abf)}-\mathrm{E}[\Delta A^{(abf)}]|]\\&\leqslant\mathrm{E}[|\Delta A^{(abf)}-\mathrm{E}[\Delta A^{(abf)}]|^2]^{1/2}\\&=\mathrm{SD}[\Delta A^{(abf)}].\end{aligned}$$

In the Appendix we derive the estimate

$$\mathrm{SD}[\Delta A^{(abf)}]\approx(\xi_b-\xi_a)\frac{\sigma}{K^{1/2}}(1+2\kappa)^{1/2}, \tag{17}$$

where $\sigma^2=\mathrm{Var}[F_\xi]$ and κ is the correlation length[40] of the series $\{F_\xi(t_m)\}_{m=1}^K$. From this equation it follows that the standard deviation of $\Delta A^{(abf)}$ decreases as $K^{-1/2}$ and increases linearly with σ.

2. Error in fast growth

a. Error in $\Delta A_N^{(\mathrm{J})}$. Zuckerman and Woolf[22,23] have recently provided asymptotic expansions in integer powers of $1/N$ for the systematic bias and variance of $\Delta A_N^{(\mathrm{J})}$. The coefficients of the expansions depend on the moments of $\exp(-\beta W)$. More specifically, assuming that the mean $\hat\mu$, variance $\hat\sigma^2$, and third central moment $\hat\mu_3$ of $\exp(-\beta W)$ are finite, Zuckerman and Woolf prove that

$$\mathrm{E}[\Delta A_N^{(\mathrm{J})}]-\Delta A=\frac{\phi_1}{\beta N}+\frac{\phi_2}{\beta N^2}+\mathcal{O}\left(\frac{1}{N^3}\right), \tag{18}$$

$$\mathrm{Var}[\Delta A_N^{(\mathrm{J})}]\approx\frac{\chi_1}{\beta^2N}+\mathcal{O}\left(\frac{1}{N^2}\right) \tag{19}$$

with

$$\phi_1=\hat\sigma^2/(2\hat\mu^2),\quad \phi_2=-(4\hat\mu\hat\mu_3-9\hat\sigma^4)/(12\hat\mu^4),$$

$$\chi_1=\hat\sigma^2/\hat\mu^2.$$

In practice, the direct use of Eqs. (18) and (19) is problematic unless the standard deviation σ_W is small. The reason is that these estimates require an accurate evaluation of the moments of $\exp(-\beta W)$, or, equivalently, the integral of $\exp(-k\beta W)P(W)$, for $1\leqslant k\leqslant 3$. When σ_W is much larger than k_BT, the maximum of $\exp(-k\beta W)P(W)$ will be several standard deviations away from $\overline{W}$. As the lower tail of $P(W)$ is rarely sampled, a large number of trajectories will be needed to compute the coefficients in Eq. (19) with satisfactory accuracy.

If the distribution of W is Gaussian explicit expressions for the moments $\hat\mu$, $\hat\sigma^2$, and $\hat\mu_3$ are readily known.[41] Then

$$\phi_1=\frac{\eta^2}{2},\quad \phi_2=-\frac{4\eta^2+3}{12}\eta^4,$$

$$\chi_1=\eta^2\quad\text{with}\quad \eta^2=e^{\beta^2\sigma_W^2}-1. \tag{20}$$

This leads to

$$\mathrm{E}[\Delta A_N^{(\mathrm{J})}]-\Delta A=\frac{1}{2\beta}\frac{\eta^2}{N}-\frac{1}{2\beta}\frac{4\eta^2+3}{6}\left(\frac{\eta^2}{N}\right)^2+\mathcal{O}\left(\frac{1}{N^3}\right), \tag{21}$$

$$\mathrm{Var}[\Delta A_N^{(\mathrm{J})}]\approx\frac{1}{\beta^2}\frac{\eta^2}{N}+\mathcal{O}\left(\frac{1}{N^2}\right). \tag{22}$$

For $\eta^2\ll N$, the following leading order estimates are obtained:

$$\mathrm{E}[\Delta A_N^{(\mathrm{J})}]-\Delta A\approx\frac{1}{2\beta}\frac{e^{\beta^2\sigma_W^2}-1}{N}, \tag{23}$$

$$\mathrm{SD}[\Delta A_N^{(\mathrm{J})}] \approx \frac{1}{\beta}\left(\frac{e^{\beta^2\sigma_W^2}-1}{N}\right)^{1/2}. \tag{24}$$

The application of Eqs. (23) and (24) requires some caution. For fixed N there exists only a limited (and often small) interval $0<\beta\sigma_W \leqslant C(N)$ for which Eqs. (23) and (24) are valid. For fixed and large widths σ_W, the leading order estimates represent viable approximations for only a large number of trajectories. This limitation was already reported by Zuckerman and Woolf[22] and is confirmed numerically in Secs. II C and IV.

b. Error in $\Delta A_N^{(\mathrm{G})}$. As was already pointed out, the estimator $\Delta A_N^{(\mathrm{G})}$ defined in Eq. (12) is unbiased if the values $\{W_1,\ldots,W_N\}$ are sampled from a Gaussian distribution. Furthermore, an exact expression of $\mathrm{Var}[\Delta A_N^{(\mathrm{G})}]$ is available.[38] Provided that the works are uncorrelated, and $\mathrm{Var}(\langle W\rangle_N)$ and $\mathrm{Var}(s^2)$ are uncorrelated, it follows that

$$\mathrm{Var}[\Delta A_N^{(\mathrm{G})}] = \frac{\sigma_W^2}{N} + \frac{\beta^2\sigma_W^4}{2(N-1)}. \tag{25}$$

Using Eqs. (22) and (25) and a Taylor expansion, we obtain

$$\begin{aligned}
&\mathrm{Var}[\Delta A_N^{(\mathrm{J})}] - \mathrm{Var}[\Delta A_N^{(\mathrm{G})}] \\
&\approx \left[\frac{\sigma_W^2}{N} + \frac{\beta^2\sigma_W^4}{2N} + \frac{(\beta^4\sigma_W^6)}{6N} + \cdots\right] - \frac{1}{\beta^2}\frac{2\eta^2+1}{2}\left(\frac{\eta^2}{N}\right)^2 \\
&\quad - \left[\frac{\sigma_W^2}{N} + \frac{\beta^2\sigma_W^4}{2(N-1)}\right] \\
&= -\frac{\beta^2\sigma_W^4}{2N(N-1)} - \frac{1}{\beta^2}\frac{2\eta^2+1}{2}\left(\frac{\eta^2}{N}\right)^2 + \frac{\mathcal{O}(\sigma_W^6)}{N}.
\end{aligned}$$

Therefore, not only is $\Delta A_N^{(\mathrm{G})}$ unbiased, but $\mathrm{Var}[\Delta A_N^{(\mathrm{G})}]$ is always smaller than $\mathrm{Var}[\Delta A_N^{(\mathrm{J})}]$ for large N. This confirms that, for a Gaussian distribution of works, the use of $\Delta A_N^{(\mathrm{G})}$ instead of $\Delta A_N^{(\mathrm{J})}$ is advisable. Furthermore, it is possible to compare the efficiency of $\Delta A_N^{(\mathrm{G})}$ and $\Delta A^{(abf)}$ for long times τ. In this case, Woods[42] and Crooks[27] estimated that the variance σ_W^2 of the work scales as $1/\tau$. Therefore, for fixed Δt, we can assume in the long-time regime

$$\sigma_W^2 \approx \frac{\sigma_0^2}{L}, \tag{26}$$

where L is the number of time steps per trajectory and σ_0^2 is a constant that depends on the current, ξ, and initial, ξ_a, values of the reaction coordinate. Equations (25) and (26) lead to

$$\mathrm{Var}[\Delta A_N^{(\mathrm{G})}] = \frac{\sigma_0^2}{K}\left(1 + \frac{N\beta^2\sigma_0^2}{2K}\right), \tag{27}$$

where $K=NL$, i.e., the total number of time steps after the N trajectories. Taking into account Eq. (17) for standard deviation of $\Delta A^{(abf)}$:

$$\frac{\mathrm{SD}[\Delta A_N^{(\mathrm{G})}]}{\mathrm{SD}[\Delta A^{(abf)}]} \approx \frac{\sigma_0(\xi_a,\xi_b)}{(\xi_b-\xi_a)\sigma(1+2\kappa)^{1/2}}\left(1+\frac{N\beta^2\sigma_0^2}{2K}\right)^{1/2}.$$

Two regimes are found for the ratio of statistical errors depending on whether $N\beta^2\sigma_0^2/K = \beta^2\sigma_W^2$ is small or large. The transition between the two regimes occurs near $\beta\sigma_W \simeq 1$. In the best case, when σ_W is of the order of k_BT or smaller, we find

$$\frac{\mathrm{SD}[\Delta A_N^{(\mathrm{G})}]}{\mathrm{SD}[\Delta A^{(abf)}]} \approx \frac{\sigma_0(\xi_a,\xi_b)}{(\xi_b-\xi_a)\sigma(1+2\kappa)^{1/2}},$$

a system-dependent constant. Only in this optimal case is the efficiency of fast growth similar to the efficiency of ABF.

If the distribution of works is Gaussian it is possible to improve $\mathrm{Var}[\Delta A_N^{(\mathrm{G})}]$ in Eq. (27) for large $\beta\sigma_W$ by running trajectories both forward and backward (i.e., initiated at ξ_a and ξ_b). If $N/2$ trajectories are obtained in each direction[38]

$$\mathrm{Var}[\Delta A_N^{(\mathrm{G})}] = \frac{\sigma_0^2}{K}.$$

C. The harmonic oscillator

We have computed the free energy difference of changing the center of a one-dimensional harmonic oscillator of mass m and spring constant k from $c=0$ to $c=\lambda$. This is equivalent to computing the free energy associated with moving a particle in the (x,y) plane from $y_a=0$ to $y_b=1$, subject to a potential $\Phi_\lambda(x,y)=k(x-\lambda y)^2/2$.

The aim of the experiment is twofold. We want to determine the validity of the estimates given in Eqs. (23) and (24) for Gaussian distributions of works. We also want to compare in a simple experiment the efficiencies of average force methods (constrained dynamics in this case) and fast growth.

For a given temperature, the partition function is independent of y, and is given by $Z=2\pi/\beta\omega$, where $\omega=\sqrt{k/m}$ denotes the natural frequency. Therefore, the free energy difference is

$$\Delta A = -\beta^{-1}\ln\frac{Z}{Z} = 0.$$

The constrained sampling was carried out at p points along the lines $\{(x,y_i), y_i=(2i-1)/(2p)\}_{i=1}^p$. At each y_i, the Hamiltonian H_{λ,y_i} is given by

$$H_{\lambda,y_i}(x,p_x) = \frac{p_x^2}{2m} + \frac{k}{2}(x-\lambda y_i)^2.$$

For each y_i, n values of x were sampled independently from a canonical ensemble corresponding to the Hamiltonian H_{λ,y_i} at temperature T:

$$x \sim N\left(\lambda y_i, \frac{1}{\beta k}\right). \tag{28}$$

We recall that the instantaneous force acting on the y coordinate is the one which when subtracted gives a zero acceleration along y. Thus, in this particular example,

$$F_\xi = F_y = -\partial_y H(x,y) = -\partial_y\Phi_\lambda(x,y) = 2\lambda(x-\lambda y). \tag{29}$$

From Eqs. (28) and (29) it follows that

$$F_\xi \sim N\left(0, \frac{4\lambda^2}{\beta k}\right).$$

Notice that the parameter λ in the potential is used to adjust the spread of the instantaneous force acting on y. The free energy is computed by integrating the average force:

$$\Delta A_n^{(\mathrm{C})} = -\Delta\xi \sum_{i=1}^{p} \left[\frac{1}{n} \sum_{j=1}^{n} F_y(x_j, y_i) \right]. \tag{30}$$

The statistical error of the estimator $A_n^{(\mathrm{C})}$ can be calculated analytically from the standard deviation of F_y, yielding

$$\Delta A_n^{(\mathrm{C})} \sim N\left(0, \frac{2\lambda^2}{\beta p n}\right). \tag{31}$$

We observe that an increase in λ affects the performance of the method: as the potential Φ_λ becomes steeper along the x isolines, the convergence of the method worsens at a rate proportional to λ for $pn = K$ constant.

In the fast-growth method the system was isolated during the switching process. The evolution of the particle was deterministic under the Hamiltonian $H_{\lambda,y}$, where y was switched from $y=0$ to $y=1$ at a constant rate:

$$\begin{aligned} &\ddot{x} = -\frac{1}{m}\partial_x \Phi_\lambda(x(t), y(t)), \quad \ddot{y} = 0; \\ &x(0) = x_0, \quad y(0) = 0; \\ &\dot{x}(0) = v_{0x}, \quad \dot{y}(0) = \frac{1}{\tau}. \end{aligned} \tag{32}$$

The initial conditions were sampled from the canonical ensemble corresponding to $y=0$:

$$f_{\lambda,0}(x, p_x) = \frac{e^{-\beta H_{\lambda,0}(x,p_x)}}{Z} = \frac{\beta\omega}{2\pi} \exp\left[-\frac{\beta}{2}\left(\frac{p_x^2}{m} + kx^2 \right) \right],$$

leading to Gaussian distributions for $x_0 \sim N(0, 1/k\beta)$ and $v_{0x} \sim N(0, 1/m\beta)$. The initial points in the phase space (x_0, v_{0x}) were sampled independently. At the end of each trajectory, the work W_τ was computed as the energy difference between initial and final states:

$$W_\tau = \Delta E = \frac{m}{2}[|v_x(\tau)|^2 - |v_{0x}|^2] + \frac{k}{2}\{[x(\tau) - \lambda]^2 - x_0^2\}.$$

The system described by Eq. (32) can be integrated analytically. After some algebra we get

$$\begin{aligned} &x(t) = x_0 \cos(\omega t) + \frac{v_{0x} - \lambda/\tau}{\omega} \sin(\omega t) + \frac{\lambda}{\tau} t, \\ &W_\tau = m\frac{\lambda}{\tau}\left[\left(v_{0x} - \frac{\lambda}{\tau} \right)[\cos(\omega\tau) - 1] - x_0 \omega \sin(\omega\tau) \right]. \end{aligned} \tag{33}$$

W_τ is a linear combination of normal variables, and is therefore also normal with parameters

$$W_\tau \sim N\left(r(\lambda), \frac{2}{\beta} r(\lambda) \right), \quad r(\lambda) = m\left(\frac{\lambda}{\tau}\right)^2 [1 - \cos(\omega\tau)]. \tag{34}$$

Equation (34) confirms that, as W_τ is Gaussian, $\Delta A = \overline{W_\tau} - \beta\sigma_{W_\tau}^2/2$ holds true. Also, the spread in W_τ is proportional to λ.

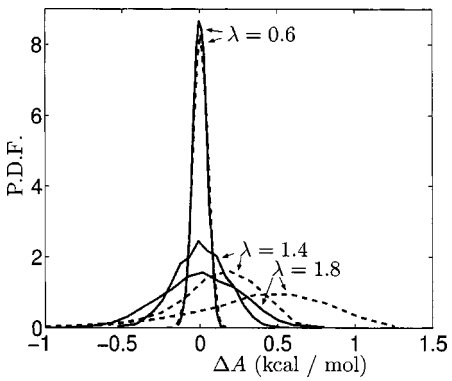

FIG. 1. Histograms of $\Delta A_N^{(\mathrm{G})}$ (solid) and $\Delta A_N^{(\mathrm{J})}$ (dashed) for $N=342$ and several values of λ. Notice that, as λ (and, accordingly, σ_W) increases, the probability density function of $\Delta A_N^{(\mathrm{J})}$ becomes right skewed and the maximum shifts to the right of the exact free energy $\Delta A = 0$. The estimator $\Delta A_N^{(\mathrm{J})}$ is thus positively biased.

We fixed the stiffness $k=2$, mass $m=0.081$, switching time $\tau=0.05$, and $\beta=1.6774$. Two sets of fast-growth computations were performed for $N=20$ and 342 (the values of β and N were chosen to make them directly comparable with the tests discussed in Sec. IV A). The work along the trajectories was obtained from Eq. (33). Subsequently, we obtained $\Delta A_N^{(\mathrm{J})}$ and $\Delta A_N^{(\mathrm{G})}$ from Eqs. (11) and (12).

For the constraint force calculation we fixed $p=50$ and set, as in the fast-growth case, $n=N=20$ and $n=N=342$ in the two different sets of computations. We computed $\Delta A_N^{(\mathrm{C})}$ from Eq. (30).

To study the statistical properties of the estimators, we obtained 4385 values of $\Delta A_N^{(\mathrm{C})}$, $\Delta A_N^{(\mathrm{J})}$, and $\Delta A_N^{(\mathrm{G})}$, respectively, for different choices of λ. Finally, we compared their efficiency for $\lambda = 0.1, 0.2, \ldots, 1.9$.

The probability density functions of $\Delta A_N^{(\mathrm{J})}$ and $\Delta A_N^{(\mathrm{G})}$ are shown in Fig. 1. $\Delta A_N^{(\mathrm{G})}$ is, as expected, unbiased, whereas $\Delta A_N^{(\mathrm{J})}$ has a systematic bias (the expected value is shifted to the right of the exact free energy $\Delta A = 0$). The bias increases as λ (and, accordingly, σ_W) increases.

The standard deviation of $\Delta A_N^{(\mathrm{J})}$ is detailed in Fig. 2(a), along with the first order estimate in Eq. (24). As has already been pointed out in Sec. II B 2 a, for each N there exists a window $0 < \beta\sigma_W \leqslant C(N)$, where the estimate is accurate. For $N=20$, we observe that Eq. (24) is valid for $\lambda < 0.5$, which corresponds to $\beta\sigma_W \simeq 0.9$. For $N=342$, Eq. (24) holds for a somewhat larger range of λ ($\lambda < 0.8$, which corresponds to $\beta\sigma_W \simeq 1.46$).

In Fig. 2(b) we show the standard deviation of $\Delta A_N^{(\mathrm{G})}$. For both values of N, we observe the two regimes anticipated in Eq. (25):

$$\mathrm{SD}[\Delta A_N^{(\mathrm{G})}] \approx \begin{cases} \dfrac{\sigma_W}{N^{1/2}} & \text{if } \beta\sigma_W \ll 1, \\ \dfrac{\sigma_W}{N^{1/2}}\left(1 + \dfrac{\beta^2\sigma_W^2}{2} \right)^{1/2} & \text{if } \beta\sigma_W \gg 1. \end{cases}$$

We also notice that for $N=342$, $\mathrm{SD}[\Delta A_N^{(\mathrm{G})}]$ is markedly smaller than $\mathrm{SD}[\Delta A_N^{(\mathrm{J})}]$.

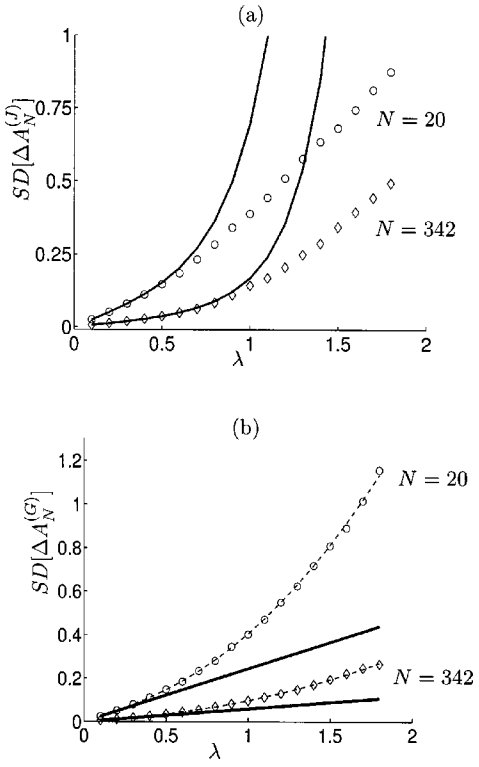

FIG. 2. (a) Standard deviation of $\Delta A_N^{(J)}$ as a function of λ for $N=20$ (circles) and $N=342$ (diamonds). The solid lines represent the first-order estimate (24). For $N=20$, the formula (24) is accurate until $\lambda=0.5$, where $\beta\sigma_W \simeq 0.9$. For $N=342$, the threshold increases to $\lambda=0.8$, where $\beta\sigma_W \simeq 1.46$. (b) Standard deviation of $\Delta A_N^{(G)}$ as a function of λ for $N=20$ (circles) and $N=342$ (diamonds). Solid thick lines represent the estimate $\sigma_W/N^{1/2}$, whereas dashed light lines represent the estimate $(\sigma_W/N^{1/2})[1+(\beta^2\sigma_W^2)/2]^{1/2}$.

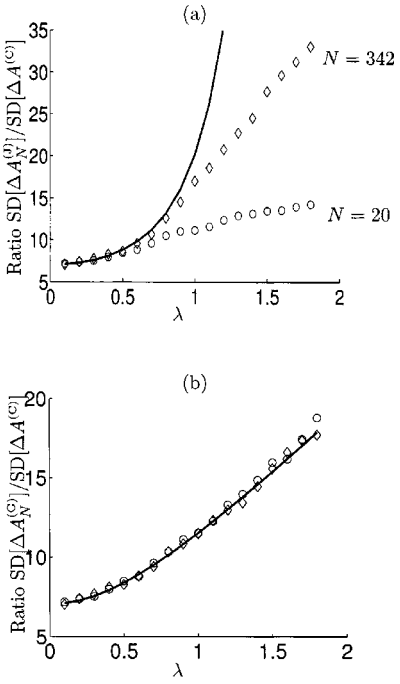

FIG. 3. (a) The ratio $SD[\Delta A_N^{(J)}]/SD[\Delta A^{(C)}]$ as a function of λ for $N=20$ (circles) and $N=342$ (diamonds). As $N\to\infty$, the ratio converges to the limit $(\sqrt{p/2\beta})\sqrt{(e^{\beta^2\sigma_{W-1}^2})}/\lambda$, represented by the solid line. (b) The ratio $SD[\Delta A_N^{(G)}]/SD[\Delta A^{(C)}]$ as a function of λ for $N=20$ (circles) and $N=342$ (diamonds). As expected, the ratio is independent of N and is approximately equal to the function $(\sigma_W/\lambda)(1+\beta^2\sigma_W^2/2)^{1/2}(\beta p/2)^{1/2}$ represented by the solid line.

In Figs. 3(a) and 3(b) we show that the ratios $SD[\Delta A_N^{(J)}]/SD[\Delta A_N^{(C)}]$ and $SD[\Delta A_N^{(G)}]/SD[\Delta A_N^{(C)}]$ increase with λ. In other words, the constraint force technique performs increasingly better than both fast-growth estimators when the spreads of the instantaneous force F_y and the work W increase.

The comparison of statistical errors for fixed λ and increasing N (increasing computational cost) is also of interest. Figure 3(a) reveals that the ratio $SD[\Delta A_N^{(J)}]/SD[\Delta A_N^{(C)}]$ increases until it reaches a well defined limit. Indeed, as $N\to\infty$ the estimate in Eq. (24) becomes accurate. The limit is given by

$$\lim_{N\to\infty}\frac{SD[\Delta A_N^{(J)}]}{SD[\Delta A_N^{(C)}]}=\lim_{N\to\infty}\frac{1}{\beta}\left(\frac{e^{2\beta r(\lambda)}-1}{N}\right)^{1/2}\left(\frac{\beta p N}{2\lambda^2}\right)^{1/2}$$
$$=\sqrt{\frac{p}{2\beta}}\frac{\sqrt{e^{2\beta r(\lambda)}-1}}{\lambda},$$

a function that grows exponentially in λ. By contrast, the ratio $SD[\Delta A_N^{(G)}]/SD[\Delta A_N^{(C)}]$, shown in Fig. 3(b), is independent of N. The constant

$$\frac{SD[\Delta A_N^{(G)}]}{SD[\Delta A_N^{(C)}]}=\frac{\sigma_W}{N^{1/2}}\left(1+\frac{\beta^2\sigma_W^2}{2}\right)^{1/2}\left(\frac{\beta p N}{2\lambda^2}\right)^{1/2}$$
$$=\frac{[pr(\lambda)]^{1/2}}{\lambda}[1+\beta r(\lambda)]^{1/2}$$

is linear in λ.

III. METHODS

To assess the performance of the ABF and fast growth methods we studied two test cases. One example involved calculating the potential of mean force for the rotation of the C–C bond in 1,2-dichloroethane (DCE) dissolved in water. In the second example, the potential of mean force for the transfer of fluoromethane (FMet) across a water-hexane interface was obtained. Both test cases have been studied before.[20,21,24,43]

The first system consisted of one DCE molecule surrounded by 343 water molecules, all placed in a cubic box whose edge length was 21.73 Å. This yielded a water density approximately equal to 1 g/cm^3. The second system contained one FMet molecule and a lamella of 486 water molecules in contact with a lamella of 83 hexane molecules. This system was enclosed in a box, with x,y dimensions equal to 24×24 Å^2 and z dimension, perpendicular to the water-hexane interface, equal to 150 Å. Thus, the system contained one liquid-liquid interface and two liquid-vapor interfaces. The same geometry was used in a series of previous studies

TABLE II. Summary of ABF calculations performed for the test cases.

Test	$[\xi_a,\xi_b]$	Δt	Number of windows	Overlapping	Bin size	Length of trajectory per bin	Total number of steps	Samples discarded
DCE	[0, 180] (deg)	1 (fs)	5	Yes	5 (deg)	0.4 (ns)	2×10^6	5%
FMet	[−15, 10] (Å)	2 (fs)	5	No	0.2 (Å)	2.5 (ns)	6.25×10^6	2%

on the transfer of different solutes across a water-hexane interface.[11,44] In both cases, periodic boundary conditions were applied in the three spatial directions.

Water-water interactions were described by the TIP4P model.[45] The models of DCE and FMet were described in detail previously.[24,25] Interactions between different components of the system (the solute, water, and hexane) were defined from the standard combination rules.[46] All intermolecular interactions were truncated smoothly with a cubic spline function between 8.0 and 8.5 Å. Cutoff distances were measured between carbon atoms of DCE and FMet, oxygen atoms of water, and united atoms of hexane.

The equations of motion were integrated using the velocity Verlet algorithm with a 1 fs time step for DCE and a 2 fs time step for FMet. The temperature was kept constant at 300 K using the Martyna *et al.* implementation[47] of the Nosé–Hoover algorithm.[48,49] This algorithm allows for generating configurations from a canonical ensemble. Bond lengths and bond angles of water and hexane molecules were kept fixed using RATTLE.[35]

For DCE in water, the Cl–C–C–Cl torsional angle ξ was taken as the reaction coordinate. For the transfer of FMet across the water-hexane interface, ξ was defined as the z component of the distance between the centers of mass of the solute and the hexane lamella.

The sets of calculations performed for both systems are summarized in Tables II and III. In order to make a fair comparison between the efficiency of different methods, we took roughly the same number of time steps to generate the profiles $A(\xi)$ in all cases. Specifically, we fixed the total computational cost to roughly 2×10^6 time steps for the DCE test and 6×10^6 time steps for the FMet test. The time steps devoted to generating initial configurations for fast growth trajectories were not included in the comparison.

The initial configurations for fast growth trajectories were generated by a single run with ξ constrained at ξ_a. One configuration was saved every 2500 steps. For each configuration, the velocities were resampled according to the Maxwell–Boltzmann probability distribution. Next, one step of the velocity Verlet algorithm was executed to obtain new positions and velocities. In this way, we ensured that different initial configurations for fast growth were completely uncorrelated. Finally, the trajectories were run independently in parallel processors (no relaxation was used between consecutive switches), with a constant speed $\dot{\xi}$.

In the DCE test, six sets of calculations were performed. The first set yielded $A(\xi)$ using ABF. We used five overlapping windows (see Table IV) over the interval [0°, 180°]. The MD trajectory in each window was 0.4 ns long. Force statistics were collected in bins 5° wide. The initial 5% of the samples in each bin were used exclusively to compute the biasing force, and were not used for computing the final $A(\xi)$.

The remaining five calculations were performed using the fast-growth method for different switching times τ. We computed the profile $A(\xi)$ corresponding to the fastest and the slowest growths ($\tau=5$ and 97.5 ps, respectively). The remaining data were used to study in detail the dependence of σ_W on ξ and τ.

In the FMet test, three sets of calculations were performed, one for ABF and two for the fast growth method for two different switching times τ. For ABF, we used five nonoverlapping windows (detailed in Table IV) over the interval [−15, 10] Å. The MD trajectory in each window was 2.5 ns long. Force statistics were collected in bins 0.2 Å wide. In this case the initial 2% of the samples in each bin was discarded when computing $A(\xi)$.

For fast growth, a total of 90 trajectories for $\tau=640$ ps and two trajectories for $\tau=5.25$ ns were obtained.

TABLE III. Summary of fast growth calculations performed for the test cases.

Test	$[\xi_a,\xi_b]$	Δt	τ	Number of trajectories	Number of blocks	Steps per block
DCE	[−10, 180]	1 (fs)	5 (ps)	1026	3	1.71×10^6
			7.5 (ps)	600	—	—
			22.5 (ps)	240	—	—
			52.5 (ps)	109	—	—
			97.5 (ps)	140	7	1.95×10^6
FMet	[−15, 10]	2 (fs)	0.64 (ns)	90	5	5.76×10^6
			5.25 (ns)	2	1	5.76×10^6

IV. RESULTS AND DISCUSSION

A. Rotation of the C–C bond in DCE dissolved in water

In Fig. 4 we show the free energy profile for the rotation of DCE around the Cl–C–C–Cl torsional angle. This profile, obtained using ABF, is in excellent agreement with the previously calculated reference curve.[21] The free energies for the *gauche* and *trans* conformations in water are nearly the same. In contrast, in the gas phase the *trans* conformation is favored by 1.1 kcal/mol.[24,43] This means that, compared to the *trans* rotamer, the *gauche* conformation is stabilized in the aqueous environment by 1.4 kcal/mol. This can be explained by favorable interactions between the permanent di-

TABLE IV. Setup for windows used in ABF.

Test	Units	Window 1	Window 2	Window 3	Window 4	Window 5
DCE	deg	[0, 46]	[26, 82]	[62, 118]	[107, 154]	[134, 180]
FMet	Å	[−15, −10]	[−10, −5]	[−5, 0]	[0, 5]	[5, 10]

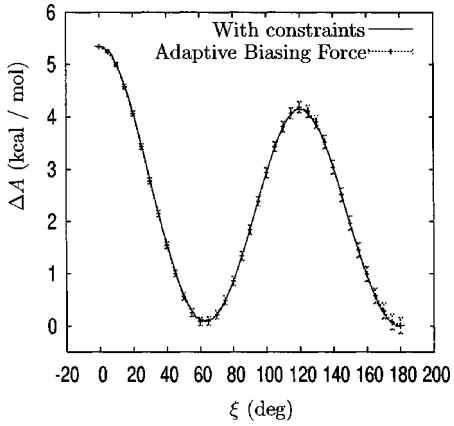

FIG. 4. Free energy profile of the torsional angle of DCE in bulk water calculated using the method of average force for constrained simulations and ABF.

pole of DCE in the *gauche* state and the surrounding water. These interactions are absent if DCE is in the *trans* conformation because, by symmetry, this state has no dipole moment. The free energy barrier was found to be equal to 4.2 kcal/mol, approximately 0.7 kcal/mol higher than the same barrier in the gas phase. The error bars were computed using Eq. (17). Its larger value is 0.15 kcal/mol.

The results obtained by fast growth were also satisfactory. For $\tau=5$ ps, three independent profiles of $N=342$ trajectories were generated using the estimators $\Delta A_N^{(\mathrm{J})}$ and $\Delta A_N^{(\mathrm{G})}$. For the sake of clarity we show only one profile for each estimator in Fig. 5(a). We computed the error bars as the standard deviation of the three independent estimates of $\Delta A_N^{(\mathrm{J})}$ and $\Delta A_N^{(\mathrm{G})}$. The maximum error obtained along the profile was 0.11 kcal/mol for $\Delta A_N^{(\mathrm{J})}$ and 0.23 kcal/mol for $\Delta A_N^{(\mathrm{G})}$.

Again, only one of the profiles for $\Delta A_N^{(\mathrm{J})}$ and one for $\Delta A_N^{(\mathrm{G})}$ are shown for $\tau=97.5$ in Fig. 5(b), with error bars obtained calculating the standard deviation of seven independent estimates. The maximum uncertainty was found to be 0.14 kcal/mol for $\Delta A_N^{(\mathrm{J})}$ and 0.12 kcal/mol for $\Delta A_N^{(\mathrm{G})}$. We conclude that both ABF and fast growth techniques show a similar efficiency in this test.

We next analyzed the values of W obtained for five different switching times. The Gaussian fits in Fig. 6(a) show that the work can be considered as sampled from Gaussian distributions with parameters $\overline{W}$ and σ_W^2 dependent on ξ and τ. As expected, the nonequilibrium effects propagate along the trajectory, causing σ_W to increase as ξ increases.

From Fig. 6(b), we observe that decreasing the switching time has the same effect. Moreover, we observe that σ_W^2 scales as $1/\tau$ for switching times τ longer than 22.5 ps:

$$\sigma_W^2 \approx \frac{\rho_0^2}{\tau} \quad \text{for} \quad \tau \geqslant 22.5 \text{ ps},$$

and ρ_0^2 is a constant that depends on the current, ξ, and initial, ξ_a, values of the reaction coordinate. Indeed, this confirms the scaling given in Eq. (26) for the slow-growth regime with

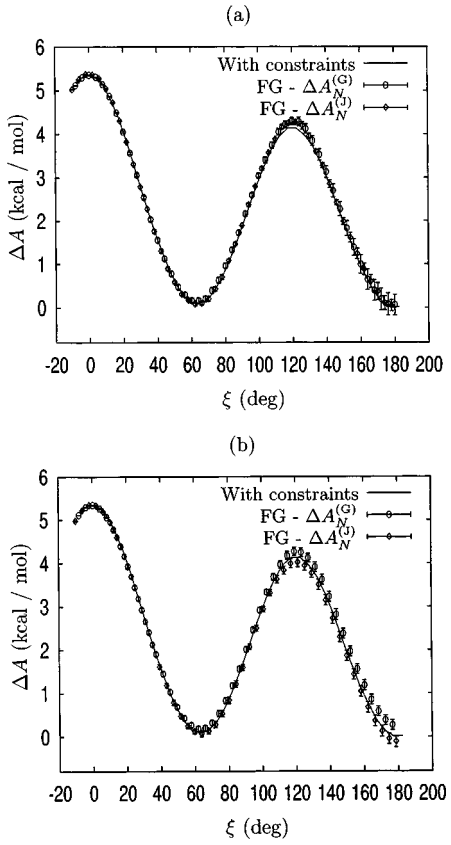

FIG. 5. (a) Free energy profile of DCE in water using the method of average force for constrained simulations vs fast growth with $N=342$ and $\tau=5$ ps. (b) Free energy profile of DCE in water using the method of average force for constrained simulations vs fast growth with $N=20$ and $\tau=97.5$ ps.

$$\sigma_0^2(\xi_a,\xi) = \frac{\rho_0^2(\xi_a,\xi)}{\Delta t}.$$

The constant $\rho_0^2(\xi_a,\xi)$ was obtained by fitting over the whole range $[-10°, 180°]$ a linear function of ξ, leading to

$$\rho_0^2 \simeq 3.31(\xi-\xi_a), \quad -10° \leqslant \xi \leqslant 180°.$$

Since W is Gaussian, the estimate in Eq. (24) can provide an alternative way of assessing the statistical error of $\Delta A_N^{(\mathrm{J})}$. Its applicability depends on the value of the variance σ_W^2. Specifically, $\{\exp[\beta^2\sigma_{W_\tau}^2(\xi)]-1\}/N$ must remain small enough along the range $[\xi_a,\xi_b]$ such that the expansion in Eq. (22) can be approximated by its first-order term. In Sec. II C (harmonic oscillator) we found numerically the following intervals of validity for this estimate:

$$N=342, \quad \beta\sigma_W \simeq 1.46,$$

$$N=20, \quad \beta\sigma_W \simeq 0.9.$$

In the present case, we obtain from Fig. 6(b)

$$N=342, \quad \tau=5 \text{ ps}, \quad \xi=180°, \quad \beta\sigma_W \approx 2.4 \quad (>1.46),$$

$$N=20, \quad \tau=97.5 \text{ ps}, \quad \xi=180°, \quad \beta\sigma_W \approx 0.43 \quad (<0.9).$$

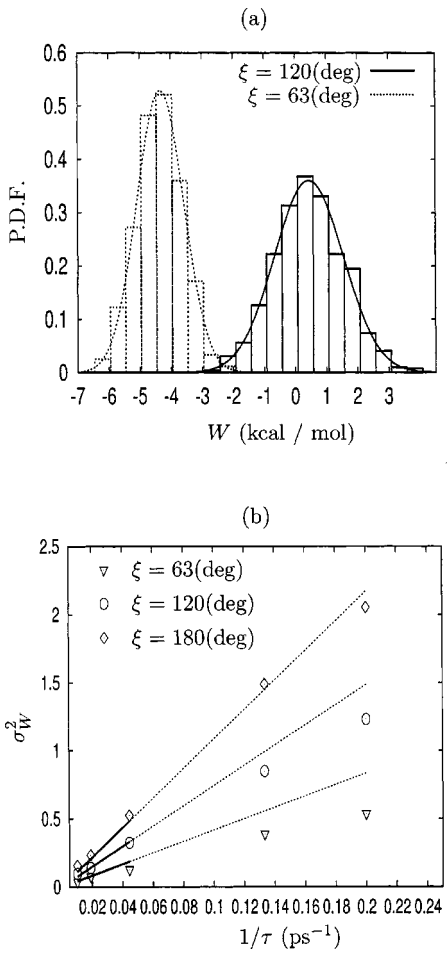

FIG. 6. (a) Histograms of the work values obtained at $\xi=63°$ and $\xi=120°$ for 1026 fast growth trajectories. Switching time $\tau=5$ ps. The Gaussian fits show that the work can be considered as sampled from Gaussian distributions. (b) Dependence of σ_W^2 on ξ and τ for fast growth in DCE. The solid lines show that σ_W^2 behaves as ρ_0^2/τ in the slow-growth regime ($\tau \gtrsim 22.5$ ps). A fit over the whole range $[-10°, 180°]$ reveals that $\rho_0^2 \simeq 3.31(\xi-\xi_a)$. The scaling does not hold for the fastest switching times (dotted lines).

It follows that we can use Eq. (24) to obtain an estimate of the statistical error only for $N=20$ and $\tau=97.5$ ps, yielding 0.1 kcal/mol at $\xi=180°$. This is in good agreement with the estimate obtained from several independent sets of trajectories earlier in this section.

B. Transfer of FMet across a water-hexane interface

The free energy profile for the transfer of FMet across a water-hexane interface obtained using ABF is shown in Fig. 7. The free energy exhibits a minimum at the interface, which is approximately 2 kcal/mol deep (compared to the free energy in bulk water). The existence of this minimum is due to the lower density at the interface between weakly interacting liquids, such as water and oil, compared to the densities in the bulk solvents. As a result, the probability of finding a cavity sufficiently large to accommodate the solute increases and the corresponding free energy cost of inserting a small, nonpolar or weakly polar solute decreases.[50] Similar free energy profiles were found for a wide range of other solutes.[11,44,51] The free energy difference between FMet in water and hexane is approximately equal to 0.5 kcal/mol, which corresponds well to the measured partition coefficient between these two liquids.[50]

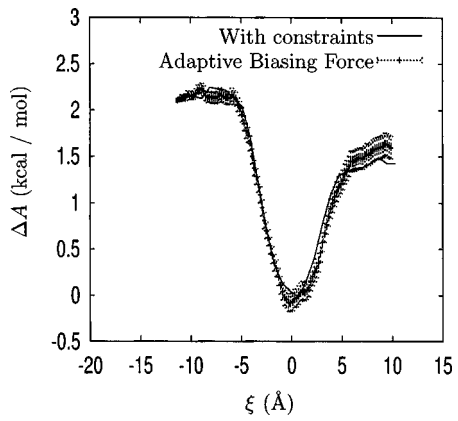

FIG. 7. Free energy profile of the transfer of FMet calculated using the method of average force for constrained simulations and ABF.

The difference between the ABF and reference curves[21] is within the error bounds given by Eq. (17). The maximum error is 0.12 kcal/mol. The profile is also in a very good agreement with the profile obtained for the same process using the particle insertion method,[50] which is highly accurate for small solutes.

In comparison, fast growth provides poor results. Figure 8(a) shows two profiles $A(\xi)$, obtained with $\Delta A_N^{(G)}$ and $\Delta A_N^{(J)}$. In both cases, the error bars represent the standard deviation obtained from five independent estimates. The uncertainty in the estimate $\Delta A_N^{(J)}(\xi)$ can exceed in some points 0.5 kcal/mol. The estimate $\Delta A_N^{(G)}(\xi)$ is even worse, as it is systematically biased for most of the interval $[\xi_a, \xi_b]$.

We have no theoretical estimate assessing the error of $\Delta A_N^{(J)}$ in this case. As pointed out in Sec. II B 2 a, expansion (19) requires an accurate computation of the moments of $\exp(-\beta W)$. However, as shown Fig. 9(a), this is not possible as the lower tail of $P(W)$ is insufficiently sampled.

The fundamental reason of the poor efficiency of fast growth is shown in Fig. 9(b). Given the computational expense of the simulation, for a relatively long switching time (only 18 trajectories), σ_W is on the order of $3k_BT$, which shows that we are still far from the slow-growth regime. This is in contrast with the DCE test, where σ_W was smaller than k_BT. In other words, for the FMet system, it is very difficult to remain close to equilibrium, i.e., perform an adiabatic switching. As a consequence, the efficiency of fast growth is much worse than ABF.

Slower runs do not help to achieve good results. In Fig. 8(b) we show the profile $A(\xi)$ obtained with $\tau=5.25$ ns and $N=2$ trajectories. Although there is a slight improvement in matching the reference free energy profile, the error remains quite large (0.5 kcal/mol).

V. SUMMARY AND CONCLUSIONS

In this paper we analyze the efficiency of two recently developed methods for calculating the free energy along a generalized coordinate in the system. One method, often

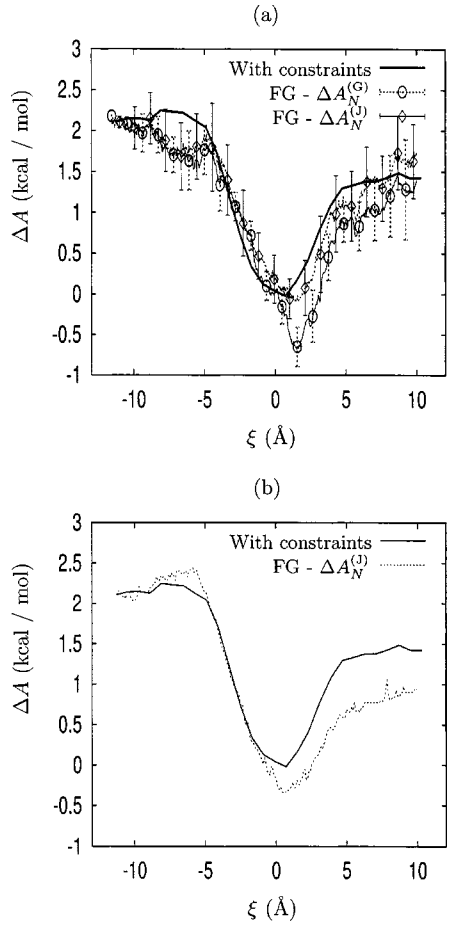

FIG. 8. Free energy profile of the transfer of FMet calculated using the method of average force for constrained simulations and fast growth with (a) $N=18$ and $\tau=640$ ps and (b) $N=2$ and $\tau=5.25$ ns.

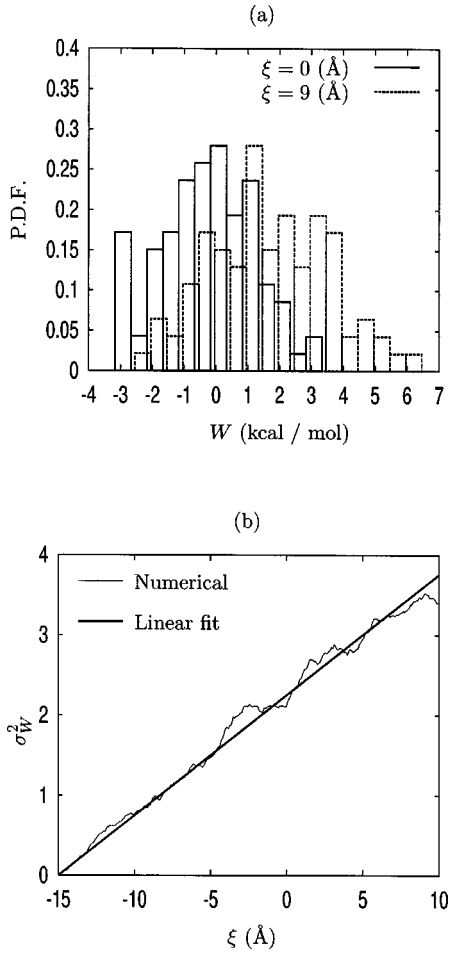

FIG. 9. (a) Histograms of the work values obtained at $\xi=0$ and $\xi=9$ (Å) from 90 fast growth trajectories. Switching time $\tau=640$ ps. (b) Dependence of σ_W^2 on ξ and linear fit for the test of (a).

called fast growth, is based on the relation given in Eq. (10), recently derived by Jarzynski.[18,19] The second method relies on thermodynamic integration of the average force acting along the reaction coordinate in an unconstrained simulation.[20,21] Interestingly, the key step in the implementation of these two rather different methods is identical—in both cases the instantaneous force acting along the reaction coordinate must be calculated. The general formula for this force in systems with single or multiple reaction coordinates has been derived recently.[20,21] In both methods the knowledge of the instantaneous force is used to modify the behavior of the system, but in a different manner. In fast growth the force is subtracted from the forces acting on the particles in the system at each time step. Thus, there is no net force acting along the reaction coordinate, which guarantees that the system evolves along this coordinate with constant, initially assigned velocity, as required in the method. This allows for generating an ensemble of nonequilibrium trajectories that can yield the average in Eq. (10). In contrast, in ABF an estimate of the *average* of instantaneous forces acting along the reaction coordinate is subtracted. This yields a Hamiltonian system which, in general, is different from the original one. In the modified system the forces acting on the reaction coordinate have approximately zero mean but the same higher moments as the forces in the original system.

The results for the two examples considered in this study—rotation of hydrated 1,2-dichloroethane around the C–C bond and transfer of fluoromethane across a water-hexane interface—reveal striking differences in the performance of the fast growth method versus the ABF method. In the DCE case, the free energy profiles obtained from both methods are in excellent agreement and coincide with the profiles previously calculated using other methods. The distribution of work performed on the system during nonequilibrium trajectories in fast growth is approximately Gaussian even for relative short switching times. This allows use of previously derived[22,23] formulas for standard deviations of the free energy difference based on both Jarzynski's[18] and Gaussian[38] estimators. These standard deviations have been compared with the corresponding standard deviations for ABF derived in this study and with standard deviations obtained from numerical analysis. All these values are similar, indicating that efficiencies of fast growth and ABF are approximately the same.

The situation is quite different in the FMet case. The free energy profile obtained from ABF is very similar to the profiles previously calculated using constrained force thermodynamic integration and the highly accurate particle insertion method. The agreement, however, is not nearly as good for

fast growth. At the same cost, the error in the calculated free energy is substantial for all, even very slow, switching times. In addition, this error can be estimated only from numerical results but not from the analytical formulas. This is because the distributions of works are not Gaussian, which violates the assumptions underlying the formulas for standard deviations given in Eqs. (24) and (27).

These results lead us to a conclusion that fast growth may not be an efficient approach to estimating free energy changes along ''physical'' reaction coordinates (defined by generalized coordinates in the system). In some cases, such as internal rotation of DCE, computationally efficient switching times can be readily chosen, for which the system remains close to equilibrium for the full length of the trajectory. Then the fast-growth method performs well but not better than ABF. Theoretical analysis of error confirms this conclusion. In other cases, even as simple as transfer of FMet across a water-hexane interface, the system is easily driven away from equilibrium. As a result, the distributions of works are broad and non-Gaussian even for relatively long switching times. In such cases, fast growth is clearly much less efficient that ABF. In addition, for non-Gaussian distributions of works no practical formula for error is available. Considering that predicting whether the system will remain close to equilibrium or not does not appear to be simple, the utility of fast growth may be limited at present. In the future, however, free energy estimates obtained from fast growth might improve through better predictions of the probability distribution of work for small values of the argument or through developing tighter bounds on the free energy without referring to the probability distribution in this poorly sampled range of work. An example of the second approach is the recent work of Lu *et al.*[52]

It is also possible to improve both ABF and fast growth by increasing the number of sample points in regions where the variance of the force is large. For ABF, this can be naturally done using windows for example. For fast growth, this is done by using a nonconstant switching velocity $v_\xi^0(t)$. By choosing a smaller (larger) $v_\xi^0(t)$ in regions where the variance of the force is large (small) it is possible to reduce statistical error without increasing the computational cost. Note, however, an important difference between ABF and fast growth. In ABF, after the simulation is completed, it is always possible to obtain additional samples in regions where the sampling is insufficient. On the contrary, for fast growth, we need to determine beforehand $v_\xi^0(t)$. For example, a few runs with $d\xi/dt$ constant can be used to estimate the variance of the force acting on ξ. From these data, the optimal $v_\xi^0(t)$ can be estimated. However, once the fast growth calculation has started, it is not possible to change $v_\xi^0(t)$.

As we have already pointed out, ABF is preferred over the probability distribution method because it yields uniform or nearly uniform sampling of the reaction coordinate. However, in many cases it may not have significant advantages over thermodynamic integration based on constrained simulations, especially if there are no concerns about nonergodicity in sampling orthogonal degrees of freedom. Nevertheless, compared to constrained force simulations, ABF may have other advantages for both thermodynamic and dynamic calculations. For example, instead of subtracting the average force along the reaction coordinate one might subtract only a fraction α. This would create a system in which relative stabilities of different states remain the same but the barriers are reduced by α. This, in turn, increases the probability of transitions between different states. Alternatively, one can substitute the average force by other, arbitrary chosen forces acting along the reaction coordinate. This new force might, for example, steer the system toward specific states. These applications of ABF will be explored in the future.

ACKNOWLEDGMENT

This paper was supported by the NASA Exobiology Program.

APPENDIX: STATISTICAL ERROR IN ADAPTIVE BIASING FORCE

We start by relating the global average of the forces obtained along the simulation, denoted as μ, with the averages μ_i in each bin:

$$\mu = \mathrm{E}[F_\xi] = \lim_{K\to\infty} \frac{\Sigma_{m=1}^{K} F_\xi(t_m)}{K} = \lim_{K\to\infty} \frac{\Sigma_{i=1}^{p}\Sigma_{i=1}^{n_i} F_\xi^u(t_l^i)}{K} = \lim_{K\to\infty} \sum_{i=1}^{p} \langle F_\xi^u \rangle_{\xi_i,n_i} P(\xi_i) = \frac{\Sigma_{i=1}^{p}\mu_i}{p}.$$

This yields

$$\mathrm{E}[\Delta A^{(abf)}] = -\Delta\xi \sum_{i=1}^{p} \mu_i = -\Delta\xi p\mu = -\Delta\xi \sum_{i=1}^{p} \mu. \tag{A1}$$

With similar arguments, the following identity follows for the global variance of the forces:

$$\sigma^2 = \mathrm{Var}[F_\xi] = \frac{\Sigma_{i=1}^{p}\sigma_i^2 + (\mu-\mu_i)^2}{p}. \tag{A2}$$

The fluctuations on the final estimate of the free energy can be expressed as

$$\mathrm{E}[|\Delta A^{(abf)}-\mathrm{E}[\Delta A^{(abf)}]|^2]=\mathrm{E}\left[\left|\Delta\xi\sum_{i=1}^{p}(\langle F_\xi\rangle_{\xi_i,n_i}-\mu)\right|^2\right] \quad [\text{using Eq. (A1)}]$$

$$=(\Delta\xi)^2\sum_{i,j=1}^{p}\sum_{l=1}^{n_i}\sum_{k=1}^{n_j}\frac{1}{n_i n_j}\mathrm{E}\{[F_\xi(t_l^i)-\mu][F_\xi(t_k^i)-\mu]\} \tag{A3}$$

$$=(\Delta\xi)^2\left(\sum_{i=1}^{p}\sum_{l=1}^{n_i}\frac{1}{n_i^2}\mathrm{E}\{[F_\xi(t_l^i)-\mu]^2\}+\sum_{\substack{i,j=1;l=1;k=1\\ i\neq j \text{ or } l\neq k}}^{p;n_i;n_j}\mathrm{E}\{[F_\xi(t_l^i)-\mu][F_\xi(t_k^j)-\mu]\}\right). \tag{A4}$$

The sum in Eq. (A3) can be rewritten as

$$\sum_{i=1}^{p}\sum_{l=1}^{n_i}\frac{1}{n_i^2}\mathrm{E}\{[F_\xi(t_l^i)-\mu]^2\}=\sum_{i=1}^{p}\frac{\sigma_i^2+(\mu-\mu_i)^2}{n_i}. \tag{A5}$$

The sum in Eq. (A4) contains all the correlations along the simulation:

$$\sum_{\substack{i,j=1;l=1;k=1\\ i\neq j \text{ or } l\neq k}}^{p;n_i;n_j}\mathrm{E}\{[F_\xi(t_l^i)-\mu][F_\xi(t_k^j)-\mu]\}$$

$$=\sum_{\substack{s,r=1\\ s\neq r}}^{K}\frac{1}{n_{I(s)}n_{I(r)}}\mathrm{E}\{[F_\xi(t_s)-\mu][F_\xi(t_r)-\mu]\}, \tag{A6}$$

where $I(s)$ denotes the bin where the force $F_\xi(t_s)$ was collected.

The numerical evaluation of Eq. (A6) may be extremely lengthy. However, the approximation

$$\frac{1}{n_i}\approx\frac{p}{K}$$

turns out to be valid if K is sufficiently large such that the probability distribution $P(\xi)$ is close to uniform. This yields the following approximation:

$$\mathrm{E}[|\Delta A^{(abf)}-\mathrm{E}[\Delta A^{(abf)}]|^2]$$

$$\approx(\Delta\xi)^2\left[\frac{p}{K}\sum_{i=1}^{p}[\sigma_i^2+(\mu-\mu_i)^2]+\frac{p^2}{K^2}\right.$$

$$\left.\times\sum_{\substack{s,r=1\\ s\neq r}}^{K}\mathrm{E}\{[F_\xi(t_s)-\mu][F_\xi(t_r)-\mu]\}\right]. \tag{A7}$$

Assuming that the series of forces $\{F_\xi(t_m)\}_{m=1}^{K}$ is stationary, the sum of covariances can be approximated as

$$\frac{p^2}{K^2}\sum_{\substack{s,r=1\\ s\neq r}}^{K}\mathrm{E}\{[F_\xi(t_s)-\mu][F_\xi(t_r)-\mu]\}$$

$$=2\frac{\sigma^2p^2}{K^2}\sum_{s=1}^{K-1}(K-s)\rho_s,$$

where ρ_s denotes the autocorrelation coefficient of the forces for a lag s. Now, if K is much larger than the maximum lag for which $\rho_s\neq 0$,

$$\frac{p^2}{K^2}\sum_{s=1}^{K-1}(K-s)\rho_s=\frac{p^2}{K}\sum_{s=1}^{K-1}\left(1-\frac{s}{K}\right)\rho_s$$

$$\approx\frac{p^2}{K}\sum_{s=1}^{\infty}\rho_s=\frac{p^2}{K}\kappa,$$

where κ is the correlation length of the series.[40] If we further take into account Eq. (A2), we are led to the approximation

$$\mathrm{SD}[\Delta A^{(abf)}]\approx\Delta\xi\left[\frac{p^2}{K}\sigma^2+2\sigma^2\frac{p^2}{K}\kappa\right]^{1/2}$$

$$=(\xi_b-\xi_a)\frac{\sigma}{K^{1/2}}(1+2\kappa)^{1/2}. \tag{A8}$$

[1] D. D. Frantz, D. L. Freeman, and J. D. Doll, J. Chem. Phys. **93**, 2769 (1990).
[2] B. J. Berne and J. E. Straub, Curr. Opin. Struct. Biol. **7**, 181 (1997).
[3] T. J. H. Vlugt, M. G. Martin, B. Smit, J. I. Siepmann, and R. Krishna, Mol. Phys. **94**, 727 (1998).
[4] W. Janke, Physica A **254**, 164 (1998).
[5] S. Huo and J. E. Straub, Proteins **36**, 249 (1999).
[6] D. Frenkel and B. Smit, *Understanding Molecular Simulations* (Academic, San Diego, 2002).
[7] E. M. Boczko and C. L. Brooks III, Science **269**, 393 (1995).
[8] A. Mitsutake and Y. Okamoto, J. Chem. Phys. **112**, 10 638 (2000).
[9] P. A. Kollman, Chem. Rev. **93**, 2395 (1993).
[10] M. Gilson, J. Given, B. Bush, and J. McCammon, Biophys. J. **72**, 1047 (1997).
[11] A. Pohorille, M. Wilson, and C. Chipot, Prog. Colloid Polym. Sci. **103**, 29 (1997).
[12] S. W. Rick, J. Phys. Chem. B **104**, 6884 (2000).
[13] G. Hummer and A. Szabo, Proc. Natl. Acad. Sci. U.S.A. **98**, 3658 (2001).
[14] J. Aqvist, V. B. Luzhkov, and B. O. Brandsdal, Acc. Chem. Res. **35**, 358 (2002).
[15] T. Simonson, G. Archontis, and M. Karplus, Acc. Chem. Res. **35**, 430 (2002).
[16] R. W. W. Hooft, B. P. van Eijck, and J. Kroon, J. Chem. Phys. **97**, 6690 (1992).
[17] C. Bartels and M. Karplus, J. Phys. Chem. B **102**, 865 (1998).
[18] C. Jarzynski, Phys. Rev. Lett. **78**, 2690 (1997).
[19] C. Jarzynski, Phys. Rev. E **56**, 5018 (1997).
[20] E. Darve, M. Wilson, and A. Pohorille, Mol. Simul. **28**, 113 (2002).
[21] E. Darve and A. Pohorille, J. Chem. Phys. **115**, 9169 (2001).
[22] D. Zuckerman and T. Woolf, Phys. Rev. Lett. **89**, 180602 (2002).
[23] D. Zuckerman and T. Woolf (unpublished).
[24] I. Benjamin and A. Pohorille, J. Chem. Phys. **98**, 236 (1993).

[25] A. Pohorille and M. Wilson, J. Chem. Phys. **104**, 3760 (1996).
[26] D. Hendrix and C. Jarzynski, J. Chem. Phys. **114**, 5974 (2001).
[27] G. Crooks, Ph.D. thesis, Department of Chemistry, University of California at Berkeley, 1999.
[28] G. E. Crooks, J. Stat. Phys. **90**, 1481 (1998).
[29] G. E. Crooks, Phys. Rev. E **60**, 2721 (1999).
[30] G. E. Crooks, Phys. Rev. E **61**, 2361 (2000).
[31] G. M. Torrie and J. P. Valleau, J. Comput. Phys. **23**, 187 (1977).
[32] S. Kumar, D. Bouzida, R. H. Swendsen, P. A. Kollman, and J. M. Rosenberg, J. Comput. Chem. **13**, 1011 (1992).
[33] S. Kumar, J. M. Rosenberg, D. Bouzida, R. H. Swendsen, and P. A. Kollman, J. Comput. Chem. **16**, 1339 (1995).
[34] W. K. den Otter and W. J. Briels, J. Chem. Phys. **109**, 4139 (1998).
[35] H. C. Andersen, J. Comput. Phys. **52**, 24 (1983).
[36] J. Liphardt, S. Dumont, S. B. Smith, I. Tinoco, and C. Bustamante, Science **296**, 1832 (2002).
[37] F. Ritort, C. Bustamante, and I. Tinoco, Proc. Natl. Acad. Sci. U.S.A. **99**, 13544 (2002).
[38] G. Hummer, J. Chem. Phys. **114**, 7330 (2001).
[39] W. Feller, *An Introduction to Probability Theory and Its Applications*, Vol. 2 (Wiley, New York, 1971).
[40] T. Straatsma, H. Berendsen, and A. Stam, Mol. Phys. **57**, 89 (1986).
[41] J. Aitchison and J. Brown, *The Lognormal Distribution* (Cambridge University Press, London, 1963).
[42] R. H. Wood, J. Phys. Chem. **95**, 4838 (1991).
[43] A. Pohorille and M. Wilson, in *Reaction Dynamics in Clusters and Condensed Phases—The Jerusalem Symposia on Quantum Chemistry and Biochemistry*, Vol. 26, edited by J. Jortner, R. Levine, and B. Pullman (Kluwer, Dordrecht, 1993), p. 207.
[44] C. Chipot, M. Wilson, and A. Pohorille, J. Phys. Chem. B **101**, 782 (1997).
[45] W. L. Jorgensen, J. Chandrasekhar, J. D. Madura, R. W. Impey, and M. L. Klein, J. Chem. Phys. **79**, 926 (1983).
[46] W. L. Jorgensen, J. D. Madura, and C. J. Swenson, J. Am. Chem. Soc. **106**, 6638 (1984).
[47] G. J. Martyna, M. L. Klein, and M. Tuckerman, J. Chem. Phys. **97**, 2635 (1992).
[48] S. Nosé, Mol. Phys. **52**, 255 (1984).
[49] W. G. Hoover, Phys. Rev. A **31**, 1695 (1985).
[50] A. Pohorille, C. Chipot, M. New, and M. Wilson, in *Pacific Symposium on Biocomputing '96*, edited by L. Hunter and T. Klein (World Scientific, Singapore, 1996), pp. 550–569.
[51] A. Pohorille, M. New, K. Schweighofer, and M. Wilson, in *Membrane Permeability: 100 Years Since Ernst Overton*, Current Topics in Membranes, edited by D. Deamer (Academic, San Diego, 1999), pp. 49–76.
[52] N. Lu, J. Adhikari, and D. A. Kofke, Phys. Rev. E **68**, 026122 (2003).